Structural control of self-healing silica–poly(tetrahydropyran)–poly(ε-caprolactone) hybrids

Fan, Wei; Youngman, Randall E.; Ren, Xiangting; Yu, Donghong; Smedskjær, Morten Mattrup

Published in:
Journal of Materials Chemistry B

DOI (link to publication from Publisher):
10.1039/D1TB00555C

Publication date:
2021

Document Version
Accepted author manuscript, peer reviewed version

ARTICLE

Structural Control of Self-Healing Silica-Poly(Tetrahydropyran)-Poly(ε-caprolactone) Hybrids

Wei Fan[1], Randall E. Youngman[2], Xiangting Ren[1], Donghong Yu[1,*], Morten M. Smedskjaer[1,*]

Received 00th January 20xx,
Accepted 00th January 20xx

DOI: 10.1039/x0xx00000x

In some biomaterial applications, the device needs to resist cyclic loading. Recently, self-healing hybrid systems with interpenetrating network of organic and inorganic components have been discovered. In this work, we clarify the structure-mechanical property relations in a new series of silica-poly(tetrahydropyran)-poly(ε-caprolactone) (SiO_2-PTHP-PCL) materials, which were prepared through a three-step synthesis, including one-pot cationic ring-opening polymerization, sol-gel reaction, and polymer-silica cross condensation. We applied THP as the main constituent of the organic phase and achieved successful polymerization under mild conditions, while the hybrid structures were controlled by the degree of silica-crosslinking and the organic/inorganic ratio. The thermal stabilities, densities, Young's modulus as well as hardness could also be regulated through such control. Notably, we find that the hybrid materials with organic polymer content above 73% are able to self-heal induced damages, including under body temperature conditions and the mechanical properties of the self-healed material are similar to those of the fresh samples. We ascribe this primarily to the reversible intermolecular interactions and hydrogen bonding among the polymer chains. Finally, we discover that the PTHP-SiO_2 networks are stable in a simulated bio-environment although PCL underwent biodegradation. The present structural control approach could lead to the design of tailored functional hybrid materials, with potential applications within areas such as soft robotics and bone regeneration.

1. Introduction

Bioactive glasses for tissue engineering and bone regeneration have received widespread attention due to their potential in bonding to bones and stimulating bone regeneration.[1-7] However, as they are made from amorphous oxides, they feature an intrinsic disadvantage, namely high brittleness, which makes them unable to withstand sustained cyclic loading as needed for use in the human body.[8] Such bioactive hybrids are mostly applied into the transplanted articular cartilage and tissues, and in order to accommodate the motions of the human body, materials with much better flexibility and strength are needed.[9, 10] Organic-inorganic amorphous hybrids with stiff inorganic contents and soft polymers can potentially overcome this problem by offering improved functional and mechanical properties.[11-14] Distinct from a simple mixture of organic and inorganic phases, these hybrids possess inorganic-organic interpenetrating networks (IO-IPNs) at the molecular scale by having covalent bonds between the two networks. Generally, this approach has the advantage of avoiding aggregation of the different phases and enabling synergistic functions of organic polymer matrix and inorganic glass components.[13, 15-18]

1 Department of Chemistry and Bioscience, Aalborg University, 9220 Aalborg, Denmark
2 Science and Technology Division, Corning Incorporated, Corning, New York 14831, USA
*Corresponding authors. email: yu@bio.aau.dk (D.Y.), mos@bio.aau.dk (M.M.S.)
Electronic Supplementary Information (ESI) available: [details of any supplementary information available should be included here]. See DOI: 10.1039/x0xx00000x

To enable the covalent bonding between the inorganic phase and the polymeric chains, and thus obtain an IO-IPN, a coupling agent is needed, which also leads to improved mechanical performance.[18, 19] The one-pot sol-gel process has for years been the most common and successful method for preparing nanoscale networks,[20-23] although more recent alternative methods such as 3D printing and electrospinning exist.[24-26] Long time condensation and low gelation rate ensure hybrids with homogeneous structures. The formed interpenetrating inorganic-organic networks achieve synergistic functions of hybrids. Silica (SiO_2) is the typical inorganic component in hybrids with IO-IPNs due to various reasons, such as its availability, low cost, simple synthesis, stability, and bio-compatibility.[1, 2] It is usually obtained through hydrolysis of tetraethyl orthosilicate (TEOS), with the mechanical properties of silica based hybrids being affected by the formed SiO_2 structures.[27, 28]

Regarding the organic component of hybrids, polycaprolactone (PCL) has shown excellent rheological and viscoelastic properties, as well as biodegradation *in vivo*.[29, 30] This makes PCL a strong candidate for biomedical hybrid fabrication. Based on the work of Jones *et al.*,[31] we here propose that tetrahydropyran (THP) has the potential to be used as the main polymer source in such hybrids. Compared to tetrahydrofuran (THF) that was adopted in the work of Jones *et al.*, the additional C atom in the THP monomer could be expected to enable better tuning of the mechanical properties of hybrids. Considering its stable six-membered cyclic structure with low ring-strain, THP is generally considered to be resistant against ring-opening and thus polymerization under mild conditions.[32] As such, polyTHP (PTHP) is a very uncommon component in biomedical hybrids.[33] However, the cationic ring-opening process can possibly solve this in the presence of an epoxide ring with higher ring strain and a suitable Lewis acid (e.g., boron trifluoride diethyletherate) as a catalyst.[31, 34] In order to obtain PTHP as the main organic component and SiO_2 as the inorganic one, we selected glycidoxypropyl trimethoxysilane (GPTMS) as the organosilane coupling agent. The epoxide group in GPTMS is structurally similar to THP monomer and could therefore act as an initiator for the polymerization of THP, while the silyl group in GPTMS would simultaneously participate in the sol-gel condensation to link with the silica network, and therefore further construct the IO-IPNs as the final product. In this way, inorganic/organic composition ratio and their corresponding structures could directly determine the structure and mechanical properties of hybrids.[14]

In this work, via applying PTHP and PCL as the polymer component and silica as the inorganic one for IO-IPN hybrids, we successfully controlled their structure by

varying the total silica/polymer composition ratio, as well as the exact chemical structure of both of the two phases, and investigated the thermal stability, mechanical properties, and biodegradation for exploring their structure-mechanical property relationship. Herein, we have also systematically studied how the inorganic/organic (I/O) ratio and silica structures (by different TEOS/water ratios) affect the hybrids' structure, mechanical properties, and self-healing abilities. These results show how mechanical properties including self-healing ability can be controlled bottom-up from the molecular level. Compared with pure inorganic samples, the hybrids offered improved flexibility and self-healing properties, suggesting the potential design strategy in the future for applications of tailored IO-IPN hybrids in soft matter and biomedical fields. We envision that our findings will be important for the rational design of hybrid materials.

2. Experimental section

2.1. Materials: All chemicals, polycaprolactone diol (HO-PCL-OH) (average Mn of 530 Da), $NaHCO_3$, KBr, 2,2,6,6-Tetramethyl-1-piperidinyloxy (TEMPO), CH_3CN, tetrahydropyran (THP), (3-glycidoxypropyl) trimethoxysilane (GPTMS), boron trifluoride-diethyl ether ($BF3{\bullet}OEt_2$), tetraethylorthosilicate (TEOS), HCl, phosphate buffered saline (PBS) solution were purchased from Sigma-Aldrich, and used as received.

2.2. Synthesis of organic sol precursor: HOOC-PCL-COOH was prepared via following the existing method of oxidation of HO-PCL-OH by using TEMPO.[31]

2.3. Synthesis of organic sol: The prepared HOOC-PCL-COOH (0.5 mol) was dissolved in anhydrous tetrahydropyran (THP) at a concentration of 50 mg mL^{-1}. Then, 1 mol GPTMS was added. After continuous stirring for 30 minutes, 0.25 mol $BF3{\bullet}OEt_2$ was added into the mixture in order to catalyze the epoxide ring-opening polymerization. In our preliminary work, we added PCL-COOH as terminating agents both at the start and end of the THF and THP organic-sol processes. We found that the reaction rate was too high to remain control when adding HOOC-PCL-COOH at the end, and TEOS precursor will not mix with polymer precursor uniformly in very high viscosity solution. Consequently, we added HOOC-PCL-COOH from the beginning of the organic-sol preparation for the consistency of the experiment. This solution was stirred for 1.5 h for reaction. The high strain of the oxirane ring gave GPTMS much higher reactivity towards catalytic ring-opening than THP. Then the carboxylic acid groups in HOOC-PCL-COOH terminated the chain growth and form the structure of GPTMS-PTHP-PCL.

2.4. Synthesis of inorganic sol: TEOS, deionized water and 36 wt% hydrochloric acid (12 M HCl) were added with the molar ratio of 1: 1.8: 0.01, 1: 3.6: 0.01, and 1: 5.4: 0.01. These three mixtures were stirred vigorously to ensure that TEOS became hydrolyzed. The completion of the reaction was directly confirmed when the mixtures turned from cloudy to clear.

2.5. Synthesis of hybrids: After preparing the organic sol, the inorganic precursors (TEOS/H_2O at the molar ratio of 1/1.8, 1/3.6, 1/5.4) were mixed with the organic sol using five different ratios (in wt%) of TEOS/ HOOC-PCL-COOH, namely 10/90, 20/80, 30/70, 40/60, and 60/40. The inorganic sol was poured drop-wise into the organic sol and stirred for at least 30 minutes at room temperature to obtain a homogeneous solution. Then, the mixed sols were transferred into a cylindrical polytetrafluoroethylene (PTFE) mold and sealed for aging for 1 week at 40 ° C. Afterwards, the molds were partially opened to allow for drying over the following three weeks at 40 °C in the furnace. When all of these processes were finished, disc-shaped samples were peeled off from the containers and used for the characterization experiments. Hence, we obtained a total of 15 samples with different compositions and thus different structures. The used TEOS/water molar ratios and TEOS/PTHP-PCL mass ratios are summarized in Table S1. All of these prepared hybrids were classified into two groups (the same silica structure with different inorganic/organic (I/O) ratio and a constant I/O ratio with various silica structure). This was done to independently evaluate the effects of SiO_2 structure and I/O ratio on the hybrid structure and mechanical properties.

2.6. Infrared spectroscopy: Fourier-transform infrared (FTIR) spectroscopy was performed by using a Bruker TENSOR II along with a Bruker Platinum ATR attachment, in the range of 4000 to 400 cm^{-1}. All spectra were compiled from 64 consecutive scans and were baseline corrected using the vendor supplied software OPUS.

2.7. Solid state NMR spectroscopy: ^{29}Si magic-angle spinning (MAS) NMR data were collected with an Agilent DD2 spectrometer in conjunction with an Oxford 4.7 T widebore superconducting magnet, with a ^{29}Si resonance frequency of 39.70 MHz. Samples were powdered and loaded into 5 mm zirconia rotors with sample spinning of 5.0 kHz. Spectra were acquired using a $\pi/6$ tip angle of 2.7 μs, a recycle delay of 180 s, averaging of 400 to 1900 scans and with high-power ^{1}H decoupling during signal acquisition.

$^{1}H \rightarrow {}^{29}Si$ cross-polarization magic-angle spinning (CPMAS) NMR measurements were made on the same instrument with a 4 ms contact time between the spins, recycle delay of 5 s and signal averaging of 5500 to

33000 scans. All ^{29}Si NMR data were processed with 25 Hz apodization, referenced to tetramethylsilane at 0.0 ppm, using the GRAMS Spectroscopy Software Suite (Thermo Fisher Scientific) to plot and fit the spectra.

^{13}C MAS NMR measurements were made at 11.7 T (125.67 MHz resonance frequency) using an Agilent DD2 spectrometer and Oxford wide-bore superconducting magnet. Powdered samples were packed into 3.2 mm zirconia rotors, with sample spinning of 20.0 kHz. ^{1}H decoupled MAS NMR data were acquired by the combination of a π/4 tip angle (2.4 μs), a 90 s delay between scans and signal averaging of 800 to 2800 scans. ^{13}C NMR data were processed with 10 Hz line broadening and referenced to tetramethylsilane at 0.0 ppm. Plotting and spectral analyses were done in the GRAMS software package.

2.8. Thin layer chromatography and liquid NMR: The oxidation of HO-PCL-OH into HOOC-PCL-COOH reaction was monitored through thin-layer chromatography (TLC) on Silica Gel 60 F254 plates. The mobile phase was a mixture of acetonitrile and ethanol in a volume ratio of 9:1 and visualization was done using I_2. The oxidation of HO-PCL-OH into HOOC-PCL-COOH was confirmed by liquid-state ^{1}H NMR spectroscopy performed on a 600 MHz Bruker spectrometer. 10 mg of polymer was dissolved in 0.5 mL deuterated chloroform ($CDCl_3$). The experimental parameters were set to acquire 16 scans in the range of chemical shift from 0 to 12 ppm.

2.9. Thermal gravimetric analysis (TGA): The final inorganic vs. organic weight ratio was determined by thermal gravimetric analysis (TGA) (DSC 449C; Netzsch, Selb, Germany). The samples were run under a flow of air at the rate of 10 °C min^{-1}, from room temperature to 800 °C. Weight loss could be ascribed to the burning-out of the organic phase.

2.10. X-ray diffraction (XRD) analysis was carried out on pulverized samples at 2θ = 5° to 80° using a Panalytical Empyrean diffractometer with a Cu-K-α radiation source (λ=1.54 Å) with a Ni-filter.

2.11. Densities and the Young's modulus were conducted through Archimedes principle and ultrasonic echography, respectively.[35]

Densities of hybrids were firstly calculated here according to the equation (1)

$$\rho_{sample} = \frac{\rho_{ethonal} \times m_{sample}^{air}}{m_{sample}^{air} - m_{sample}^{ethonal}} \qquad (1)$$

Then, the Young's Modulus (E) was obtained with the equation (2)

$$E = \rho \frac{3V_L^2 - 4V_T^2}{(V_L/V_T)^2 - 1} \qquad (2)$$

2.12. Hardness: Micro-indentation measurements were performed using a Nanovea CB500 hardness tester to determine the hardness (*H*). On each sample, 20 indentations with a maximum load of 0.07 N were generated to determine *H*, with a loading duration and dwell time of both 10 seconds. The loading and unloading rate were both 0.7 N min^{-1}. Measurements were performed under laboratory conditions (temperature: 23 °C; relative humidity: 23.5%). Then hardness was calculated from the force-displacement curves using the Oliver-Pharr model as follows,

$$H = \frac{P_{max}}{A_{pml}} \quad (3)$$

$$A_{pml} = F(h_c) \quad (4)$$

$$h_c = h_{max} - h_s \quad (5)$$

$$h_s = \varepsilon \frac{P_{max}}{S} \quad (6)$$

Here, P_{max} is the peak load, h_{max} is the depth at peak load, A_{pml} is the projected contact area, h_c is the contact depth, ε is a constant depending on the indenter, and *S* is the contact stiffness.

2.13. Dynamic mechanical analysis (DMA) was carried out using TA Instruments DMA 850. The frequency was set at 1 Hz at room temperature.

2.14. Self-healing process: Cracks were created by a sharp knife and all samples were self-healed without any external stimuli. The temperature was 23 °C and the relative humidity was 23.5 %. We also performed the same experiment at body temperature conditions (37 °C).

3. Results and discussion

3.1. Hybrid synthesis

The schematic structures of pure inorganic SiO_2, physically mixed inorganic-organic hybrids (image of non-uniform dispersion of two phases), and covalently bonded hybrids are compared in **Fig. 1**. Compared with the pure bulk SiO_2 that has many cracks (Fig. 1a), hybrids without visible cracks (Fig. 1c) can be obtained upon introducing the organic polymers into the inorganic sol. A traditional mechanically mixed hybrid material easily suffers from aggregation of nanoparticles, which would inevitably affect the uniformity and decrease the mechanical reliability. In that case, inorganic network with covalently link polymer chains is an effective way to avoid aforementioned issues. The coupling agent, GPTMS applied in this experiment, due to its oxirane group, participates in the ring-opening process with THP monomers. Additionally, the –Si-OCH_3 was also hydrolyzed and bonded to silica networks through condensation process, bridging polymer chains. Thus further uniform dispersion of inorganic nanoparticles were achieved within the polymer chains, improving the

mechanical properties (Fig. 1d-e). Consequently, we prepared the hybrids through a two-pot synthesis, combining cationic ring-opening method and sol-gel process, as shown in Scheme 1.

HO-PCL-OH had firstly been oxidized into HOOC-PCL-COOH for further reaction with PTHP and functioned as a quencher of the oxonium ion intermediates, with structure confirmed in Fig. S1 and S2.[31] ^{1}H NMR- and FTIR-spectroscopy (Fig. S1 and S2), and TLC analysis were performed to confirm its molecular structure. The peaks at 3300 cm^{-1} of FTIR and broad peak from 8.0-9.5 ppm of ^{1}H NMR both confirm the conversion of HO-PCL-OH into HOOC-PCL-COOH. THP is relatively stable due to its six-membered cyclic structure, while the ring strain of oxirane in GPTMS is much higher, and as such, the epoxide ring in GPTMS is opened firstly by $BF_3 \bullet OEt_2$ initiation.[32, 34] Then, a nucleophilic attack of the oxygen of THP by BF_3 initiated the cationic ring opening polymerization and further chain elongation steps. In this way, covalent bonds were formed between GPTMS and PTHP polymer chains, thus constructing the organic copolymer with HOOC-PCL-COOH (Fig. S3a). We noted that GPTMS not only participated in the THP ring-opening reaction, but also acted as an organosilane coupling agent for connecting silica network and polymer chains. For the inorganic sol, TEOS could be hydrolyzed into Q^1, Q^2, Q^3, and Q^4 units. Here Q^n refers to a unit with n number of –O-Si neighboring groups, and Q^1 to Q^4 are thus distinguished based on the degree of condensation of –OH and/or -OEt groups,[11, 24] as schematically illustrated in Fig. S3b. [27,28] More Q^2 structures helps to ensure flexibility, while bulky three-dimensional networks are promoted by Q^4 structures. It is generally challenging to prepare crack-free class II hybrids[13, 36] with high inorganic content, but the introduction of polymer chains and crosslinkers make it possible.

3.2 Structure of hybrids

The silica molecular structures and the polymer architectures were investigated by Fourier-transform infrared (FTIR) spectroscopy, including comparisons of the FT-IR spectra of pure inorganic samples with the hybrids. The effect of varying the molar ratio of TEOS to H_2O on the silica structure is illustrated in Fig. S4. We could roughly investigate the amount of different Q^n structures.[27, 37] The band at 1038 cm^{-1} is assigned as the Si-O-Si asymmetric stretching vibration, while the peak at 946 cm^{-1} represents vibration of Si-OH groups.[27] Moreover, the peaks at 1160 and 794 cm^{-1} are ascribed to (Si-O) Q^n structures (Peaks at 1200, 970, and 820 could be ascribed to ν(Si-O)Q^3, ν(Si-O)Q^2, and ν(Si-O)Q^1).[37, 38] Upon incorporation of the organic precursor and GPTMS, more complicated structures were formed (Fig.

2a). The bands at 2930 and 1710 cm^{-1} are ascribed to the characteristic $–CH_2$ stretching and C=O stretching, respectively.[12] These peaks appear very similar in the three hybrids, since they were kept at a constant composite ratio of PCL:TEOS=7:3. The bands at 3300 cm^{-1} can be assigned to -OH stretching. Considering the silica network, the absorption peak at 1166 cm^{-1} could be identified as the Si-O-Si asymmetric stretching vibration like in the pure inorganic system. There are also new bands in the hybrids that can be ascribed to *T*-type -Si-O (where *T*-type refers to a Si atom with one $-CH_2-$ neighbor, while the other three are -O-Si).[24, 34] The peaks around 1230 cm^{-1} are due to $–Si-CH_2$ in GPTMS. Considering the Si-O vibration range, peaks around 1099 cm^{-1} could also be ascribed to –(C=O)-O- groups in the organic polymer structures. As to the specific amount of different *Q*-type (Si-O- for all four bonds) and *T*-type SiO_2 structures, we next consider the solid-state ^{29}Si NMR spectroscopy analysis.

Focusing on the samples with different degree of hydrolysis in both pure inorganic and hybrid samples, we have used ^{29}Si NMR to evaluate differences in the SiO_2 structures (e.g., extent of hydrolysis and condensation) (Fig. 2b). Three different hydrolyzed pure silica structures were observed in Fig. S5, with typical ^{29}Si chemical shifts at -92.3, -101.7, and -110.9 ppm that can be assigned to Q^2, Q^3, and Q^4 units, respectively.[11, 24, 28, 39, 40] As seen from Fig. S5 and Table 1, a higher fraction of fully cross-linked (Q^4) structures was obtained for the material with less water available for hydrolysis of the TEOS. The population differences for Q^2, Q^3 and Q^4 in each sample are small, but consistent with excess water being available to shift the silanol condensation (elimination of H_2O) back towards more Si-OH (i.e. more Q^2 and Q^3 species).

However, when mixed with the organic precursor and reacted with GPTMS, the resulting silicate network is substantially affected, as illustrated in Fig. 2b. Namely, *T*-type SiO_2 structures are present, due to GPTMS, as reflected in the more intense ^{29}Si resonances around -60 ppm.[34] Corresponding ^{29}Si chemical shifts at -50.5, -59.9, and -66.9 ppm are assigned to T^1, T^2, and T^3 units, respectively, where T^3 are fully-crosslinked polyhedra with three siloxane bonds (Si-O-Si) and one Si-C bond.[19] The partially condensed species, T^1 and T^2, contain two and one silanol group, respectively. As shown in Fig. 2b and Table 2, after condensation the highest fractions of T^3 and Q^4 units were obtained in hybrids with the ratio as $TEOS_1H_2O_{5.4}$. This interesting result suggests that more Q^2 units in the inorganic precursors, with more chain mobility, is beneficial for the subsequent condensation with GPTMS, and results in more T^3 and Q^4 structures in the final hybrid materials. The data in Fig. 1c, measured with CPMAS NMR, are not strictly quantitative due to

the nature of cross-polarization (i.e. enhancement of signal due to nearby protons), which is an issue in precise measurement of Q^4 populations. The other resonances all have sufficient organic or silanol groups, and have been shown to give fairly equal responses under these measurement conditions (data not shown). The other trend in Fig. 2b is that the general ratio of *T*-type to *Q*-type species is consistent with the intended ratio of organic to inorganic precursors. The top spectrum ($Org_{0.9}Inorg_{0.1}$) has the lowest *Q*-type signal level, while the middle spectrum ($Org_{0.4}Inorg_{0.6}$) has the highest. The other three spectra in Fig. 2b are very similar to one another due to their identical I/O ratios. For these data, the differences in synthesis are due to water content and this appears to have only a minor impact on the extent of condensation for both the *T*- and *Q*-type silanes.

The other structural feature of these hybrid materials is the nature of the organic components, which are reflected in their ^{13}C NMR spectra. Fig. 2c contains the ^{13}C decoupled MAS NMR data for all five hybrids listed above in Table 2. While highly complex due to the different organic functional groups, including those from GPTMS, PCL and PTHP, the data have several features which support the hydrolysis and condensation reactions outlined in the aforementioned treatment of the silanes, and also the polymerization schemes of THP and CL (Fig. S3). Unreacted alkoxide functional groups, due to incomplete hydrolysis of TEOS and GPTMS, would be reflected by ethoxy peaks at 18 ($-CH_3$) and 60 (OCH_2-) ppm for TEOS, and a methoxy peak around 51 ppm in GPTMS. The latter peak from methoxy groups is completely absent in all spectra, informing that all hydrolysis of methoxy groups on GPTMS was accomplished during fabrication of these hybrid materials. The other source of alkoxide peaks, ethoxy groups of TEOS, are also noticeably absent, so again very efficient hydrolysis of the alkoxysilanes. Only the $Org_{0.4}Inorg_{0.6}$ ($T_1W_{3.6}$) material shows much signal at 60 ppm, which suggests the possibility of incomplete TEOS hydrolysis in the most inorganic-rich hybrid. The lack of any appreciable signal around 18 ppm indicates that such residual ethoxide functionality is very low in all samples.

Another finding from the ^{13}C NMR data is confirmation that GPTMS has undergone complete epoxide ring opening during the polymerization of the organic fraction in these hybrids (Fig. 2d). ^{13}C resonances in the original epoxide ring of GPTMS are found at 44 and 51 ppm, and Fig. 2c indicates that none of the five hybrid materials contain any evidence of these ring carbon peaks. Furthermore, once open and reacted with the caprolactone, these resonances move to very downfield shifts of around 62 and 72 ppm, consistent with the large number of peaks in this region and the corresponding

large fraction of different ether linkages in the organic polymers.

Thermal gravimetric analysis (TGA) has been applied to measure the inorganic vs. organic weight ratios in the hybrids. Initially, we distinguish hybrids by the weight ratio of PCL to TEOS. However, the total organic content is composed of PCL, PTHP, and the organic part of GPTMS, while the SiO_2 nanoparticles and the inorganic part of GPTMS constitute the total inorganic content. The results in Fig. 2e show that the weight begins to decrease at around 230 °C for all hybrids, which was higher than 170 °C of PTHF based hybrids in the work of Jones *et al.*[31] It represents more thermal stable hybrid materials obtained with PTHP than those with PTHF, which resulted from one more C atom in each repeat unit in the polymer backbone. The steric hindrance for the rotation of C-O bond is less than that of C-C. Thus, the rigidity of PTHP polymer chains is higher than that of PTHF polymer, which is the main reason for improved thermal stability of PTHP based hybrids.[41, 42] Fig. 2e shows a comparison of weight loss vs. temperature profiles for hybrids with the same SiO_2 structure but varying PCL/TEOS weight ratio. We find that the remaining inorganic weight found at high temperature after thermal decomposition of the organic components constitute 15.0 wt%, 20.5 wt%, 22.3 wt%, 26.7 wt%, and 36.5 wt% of hybrid $Org_{0.9}Inorg_{0.1}$ to hybrid $Org_{0.4}Inorg_{0.6}$, respectively. The results are also summarized in Table 3. Additionally, hybrids with the same PCL/TEOS weight ratio feature almost identical TGA curves (Fig. S6), which should be because the organic part is the same and decomposes, while the remaining SiO_2 particles constitute 22.3 wt%.

Finally, the non-crystallinity of the hybrid materials has been tested by X-ray diffraction (XRD). Hybrids were also compared according to various silica structures (Fig. S7) and different I/O composition ratio (Fig. 2f). As depicted in Fig. 2b, no sharp diffraction peaks typical of crystalline SiO_2 are found in the hybrids, meaning no crystalline structures in the hybrids. This is due to the hydrolysis and condensation of TEOS and GPTMS, effectively preventing the crystallization of SiO_2 nanoparticles, it is also supported by the formation of covalent bonds between silica and polymer chains during reaction and sol-gel processes, resulting in the final amorphous state. Similarly, the hybrids with different SiO_2 structures but the constant organic content are also revealed to be completely amorphous. All of these XRD results are also consistent with the ^{29}Si NMR data (Fig. 1c and S7), which showed linewidths for all peaks that reflected amorphous silicate groups.

3.3. Density, Elasticity and Rheology

We next evaluated the density, Young's modulus, and hardness for the five hybrids through Archimedes principle, ultrasonic echography, and micro-indentation methods, respectively.[37] Results are summarized in Tables 4 and 5. We find that the mechanical properties (modulus, hardness) of the five hybrids are affected by the silica structure (from TEOS/water (T/W) ratio) and I/O composition ratio. On the other hand, the densities of the hybrids $Org_{0.7}Inorg_{0.3}(T_1W_{1.8})$, $Org_{0.7}Inorg_{0.3}(T_1W_{3.6})$, and $Org_{0.7}Inorg_{0.3}(T_1W_{5.4})$ are very similar, being attributed to the same organic/inorganic ratio in these hybrids. Higher silica content in the hybrids resulted in higher density, with $Org_{0.4}Inorg_{0.6}(T_1W_{3.6})$ showing the highest density among the hybrids with the same TEOS to water molar ratio. This can be understood based on the relatively higher density of pure amorphous silica (2.2 g cm^{-3}) than those of polymers. However, we note that the type of silica structure has a negligible influence on hybrid density.

Considering the variation in Young's modulus, we find that the hybrids with higher inorganic content but the same silica structures, i.e., $Org_{0.9}Inorg_{0.1}(T_1W_{3.6})$, $Org_{0.7}Inorg_{0.3}(T_1W_{3.6})$, and $Org_{0.4}Inorg_{0.6}(T_1W_{3.6})$ reveals higher Young's modulus, up to 1.68 GPa for the hybrid $Org_{0.4}Inorg_{0.6}(T_1W_{3.6})$. This is ascribed to the high network connectivity and bond strength of amorphous silica. Moreover, based on the silica structure analysis (^{29}Si NMR data), we find that the hybrid $Org_{0.7}Inorg_{0.3}(T_1W_{5.4})$ with the most T^3, Q^4 structural feature has a higher Young's modulus of 1.29 GPa compared with those of the other two hybrids ($Org_{0.7}Inorg_{0.3}(T_1W_{1.8})$ and $Org_{0.7}Inorg_{0.3}(T_1W_{3.6})$) with the same inorganic/organic ratio. As such, the elasticity of hybrids is found to be affected by both silica structure and inorganic/organic ratio, with higher inorganic content and more T^3, Q^4 structures resulting in hybrids with higher Young's modulus.

Considering the variation in hardness (H)[43,44], the results are shown in Fig. S8-10 and Table 5. The hybrid $Org_{0.9}Inorg_{0.1}$ $(T_1W_{3.6})$ is the softest among all hybrids as it has the highest organic content, while the hardness of $Org_{0.4}Inorg_{0.6}$ $(T_1W_{3.6})$ reaches 58 MPa because of its high inorganic content (36.5%). By comparing the results for hybrids $Org_{0.9}Inorg_{0.1}$ $(T_1W_{3.6})$, $Org_{0.7}Inorg_{0.3}$ $(T_1W_{3.6})$, and $Org_{0.4}Inorg_{0.6}$ $(T_1W_{3.6})$, we conclude that the hardness increases rapidly with the increase in the inorganic content. Additionally, the results also demonstrate that hybrids with the same I/O ratio but different silica structure (as controlled by the T/W ratio) also show variation in hardness. That is, hybrid $Org_{0.7}Inorg_{0.3}$ $(T_1W_{1.8})$ shows relatively lower hardness than $Org_{0.7}Inorg_{0.3}$ $(T_1W_{3.6})$ and $Org_{0.7}Inorg_{0.3}$ $(T_1W_{5.4})$. This can mainly be ascribed to the lowest amount of T^3 structures in $Org_{0.7}Inorg_{0.3}$ $(T_1W_{1.8})$ compared with the

other two. The hybrid with higher rigidity to the network reveals much higher hardness structurally. Therefore, the higher T/W ratio induces more polymerized and branched silica structures, which in turn give higher hardness.

To test the cycling loading resistance of the hybrids, we performed up to 20 cycles of indentation load-unloading experiments to the same maximum load (Fig. S9). The curves are generally well repeated and samples avoiding cracking even after 20 cycles, although there is a minor increase in the penetration depth after multiple cycles. This generally proves the stability and durability of the prepared hybrids, confirming their potential applications within, e.g. soft robots and tissue engineering.

Finally, we also tested the rheological properties of hybrids with different I/O ratios. That is, the change in storage modulus (*E'*) and loss modulus (*E''*) with time for hybrids $Org_{0.9}Inorg_{0.1}$ ($T_1W_{3.6}$), $Org_{0.7}Inorg_{0.3}$ ($T_1W_{3.6}$), and $Org_{0.4}Inorg_{0.6}$ ($T_1W_{3.6}$) at 1 Hz under room temperature. As shown in Fig. 3, $Org_{0.4}Inorg_{0.6}$ ($T_1W_{3.6}$) possesses the highest storage modulus (~300 kPa), while hybrid $Org_{0.9}Inorg_{0.1}$ ($T_1W_{3.6}$) has the lowest (~50 kPa). The change of *E'/E''* with I/O ratio demonstrates that the hybrids transform from rubber-like to glass-like behavior with the increase in inorganic fraction. Additionally, with the increment of time, both storage modulus and loss modulus of all hybrids do not change considerably, confirming the elastic stability of the hybrids.[45]

3.4. Self-healing

With good reproducibility from all six different samples based on different PCL-diCOOH/TEOS compositions (100/0 90/10, 80/20, 70/30, 60/40, 40/60), we found that the hybrids with certain organic contents are able to autonomously self-heal after mechanical damage. Autonomous self-healing materials means that no heat, artificial light or other stimulus and materials has been used to induce repair of the damage. Here, we introduced defects by a sharp cut on the top surface of the hybrids, as shown in the optical microscopy images in Fig. 4a-d. Then samples were held at room temperature without any other stimulus for 24 h. The hybrids revealed self-healing ability to varying degree, which could also be proven by the optical microscopy images in Fig. 4e-h. The samples without SiO_2 nanoparticles (Org_1Inorg_0) and the hybrid with the smallest inorganic content $Org_{0.9}Inorg_{0.1}(T_1W_{1.8})$ were perfectly re-joined and self-healed after 24 h. Moreover, we compare self-healing abilities of hybrids $Org_{0.9}Inorg_{0.1}(T_1W_{3.6})$ and $Org_{0.9}Inorg_{0.1}(T_1W_{5.4})$ in Fig. S11, which reveal well recovery after storage for 24 hours under the same conditions. Afterwards, in order to test if the mechanical properties are fully recovered after cracking and self-healing, Fig. S12 shows a typical

indentation test of the fresh sample and self-healed after 24 h. The maximum indentation depth of fresh sample is 62 μm, while that of the self-healed sample is 70 μm. However, both samples show complete load-upload curves, and the slopes of the loading and unloading curves are also similar. We thus conclude that the mechanical properties of the self-healed hybrid $Org_{0.9}Inorg_{0.1}(T_1W_{1.8})$ are only slightly impacted.

The hybrid $Org_{0.7}Inorg_{0.3}$ also underwent recovery during the same time period, although not as much pronounced as the two hybrids with lower silica content. No apparent self-healing could be observed in $Org_{0.6}Inorg_{0.4}$, as the decreasing content of organic polymer leads to weaker intermolecular forces (London dispersive forces together with dipole-dipole interactions among PTHP and PCL polymer chains) and hydrogen bonds (formed among the carboxyl groups of PCL-COOH ending groups and hydroxyl groups in silanol in SiO_2), resulted in unfavorable self-healing properties. Thus, the driving force for the autonomous self-healing is largely triggered by the above-described supramolecular interactions in the polymer phases, and the polymer fraction therefore largely control the self-healing ability in the present hybrid system, especially in terms of the hydrogen bonds in PCL-COOH.[31]

We have also confirmed that the self-healing is possible under body temperature by storing the cracked hybrid $Org_{0.9}Inorg_{0.1}(T_1W_{1.8})$ over 8 hours at 37 °C (Fig. S13). The hybrid begins to self-heal quickly as the large crack becomes narrower after 2 hours. The cracks are almost rejoined after 4 hours and totally disappeared after 8 hours.

3.5. Biodegradability

We tested the biodegradation properties of the hybrids in order to investigate their stability in a bio-like environment since PCL has been well-recognized as a biodegradable polyester in the system.[18, 29, 30] To this end, choosing hybrids representatively like mentioned above, five hybrid samples are immersed into phosphate buffered saline (PBS) solution with pH = 7.4 (A buffer solution which is widely used in biological experiments and possesses similar osmotic pressure and pH to human body fluids) for 7 days at 37 °C (Fig. S14a). The original weight of the five hybrids ($Org_{0.7}Inorg_{0.3}(T_1W_{1.8})$; $Org_{0.9}Inorg_{0.1}(T_1W_{3.6})$; $Org_{0.7}Inorg_{0.3}(T_1W_{3.6})$; $Org_{0.4}Inorg_{0.6}(T_1W_{3.6})$; $Org_{0.7}Inorg_{0.3}(T_1W_{5.4})$) was 192.1, 330.7, 319.9, 286.7, and 205 mg, respectively. No apparent visual damage was formed after 7 days immersion and the weight of hybrids became 151.7, 251.4, 253.2, 251.6, and 162.6 mg, respectively. After immersion, the weight of the hybrids thus declined

slightly, which we mainly ascribe to hydrolytic scission of the ester linkage of PCL in such aqueous situation.[9, 22] However, the bulk samples kept their original shape after immersion and avoided swelling or cracking after soaking in PBS, revealing good stability of the PTHF-SiO_2 networks in the aqueous solution. The weight loss in the samples is exclusively due to PCL, which constituted 21.03%, 23.98%, 20.85%, 12.24%, and 20.69% of total weight mass in the five samples, respectively. In order to determine any change in total inorganic/organic ratio upon immersion, the five hybrids were tested by TGA (see, Fig. 5a, d and Fig. S14b-d). The inorganic weight fraction before immersion was 22.2%, 16.2%, 20.8%, 29.4%, and 20.9%, respectively, while it changed to 27.7%, 21.4%, 26.5%, 33.3%, and 25.8%, respectively, after immersion and drying. With the increment of 20.2%, 24.4%, 21.5%, 11.7% and 19.0%, respectively (calculated through TGA changes). These calculated changing results through TGA and mass loss of bulk samples are also in good accordance. Optical microscope images of the hybrids before and after immersion are shown in Fig. 5b-c, e-f and Fig. S14-15. The surfaces of the hybrids were relatively smooth before immersion, but defects appeared after 7 days of immersion, with the appearance of small cracks in hybrids with higher inorganic content (especially in the brittle pure inorganic sample). This provides additional strong indication that PCL degraded and entered the PBS solution. Hence, shapes and volumes of samples are maintained under such circumstance but with the degradation of PCL, which is important in biomedical applications.

4. Conclusions

In summary, we have successfully prepared a novel series of SiO_2-PTHP-PCL ternary inorganic-organic hybrids through one-pot cationic ring-opening polymerization and sol-gel method. In this work, THP was successfully polymerized under a mild condition, which was very inspiring in related synthesis processes. Such an extended monomer repeat unit based PTHP hybrids improved their thermal stability and Young's modulus compared with THF based ones. In this work, we focused and systematically explored structural and mechanical influences of silica structures together with I/O compositions to these hybrids, finding that silica structures determined the molecular structures and mechanical properties of hybrids, while I/O compositions controlled densities, mechanical properties, and self-healing abilities. Moreover, the constructed PTHP-SiO_2 networks maintained desirable bio stability, without dissolving or swelling in PBS solution although with PCL biodegraded, which revealed potential in guaranteeing enough mechanical support with reasonable

bio-degradability as biomedical materials applied in tissue engineering, bone regeneration, and soft robotics.

.

Conflicts of interest

There are no conflicts to declare.

Acknowledgements

This work was supported by the China Scholarship Council (CSC No. 201904910782).

References

1 M. Colilla, A. J. Salinas and M. Vallet-Regí, Amino−Polysiloxane, *Chem.Mater*, 2006, **18**, 5676-5683.

2 P. Saravanapavan, J. R. Jones, R. S. Pryce and L. L. Hench, *J. Biomed. Mater. Res. Part A*, 2003, **66**, 110-9.

3 D. S. Brauer, *Angewandte Chemie*, 2015, **54**, 4160-81.

4 U. G. Wegst, H. Bai, E. Saiz, A. P. Tomsia and R. O. Ritchie, *Nat. mater.*, 2015, **14**, 23-36.

5 H. Shegarfi and O. Reikeras, *J. Orthop. Surg.*, 2009, **17**, 206-11.

6 Q. Fu, E. Saiz, M.N. Rahaman and A.P. Tomsia, *Adv. Funct. Mater.*, 2013, **23**, 5461-5476.

7 M. Vallet-Regi and E. Ruiz-Hernandez, *Adv. Mater.*, 2011, **23**, 5177-218.

8 M. N. Rahaman, D. E. Day, B. S. Bal, Q. Fu, S. B. Jung, L. F. Bonewald and A. P. Tomsia, *Acta biomater.*, 2011, **7**, 2355-73.

9 I. Izquierdo-Barba, A. J. Salinas and M. Vallet-Regí, *Int. J. Appl. Glass Sci.*, 2013, **4**, 149-161.

10 Q. Fu, E. Saiz and A. P. Tomsia, *Adv. Funct. Mater.*, 2011, **21**, 1058-1063.

11 E. M. Valliant, F. Romer, D. Wang, D. S. McPhail, M. E. Smith, J. V. Hanna and J. R. Jones, *Acta biomater.*, 2013, **9**, 7662-71.

12 J. J. Chung, S. Li, M. M. Stevens, T. K. Georgiou and J. R. Jones, *Chem.Mater.*, 2016, **28**, 6127-6135.

13 B. M. Novak, *Adv. Mater.*, 1993, **5**, 422-433.

14 J. R. Jones, *Acta biomater.*, 2013, **9**, 4457-86.

15 L. S. Connell, L. Gabrielli, O. Mahony, L. Russo, L. Cipolla and J. R. Jones, *Polym. Chem.* 2017, **8**, 1095-1103.

16 A. Kumar, K. M. Rao and S. S. Han, *Chem. Eng. J.*, 2017, **317**, 119-131.

17 J. J. Blaker, A. Bismarck, A. R. Boccaccini, A. M. Young and S. N. Nazhat, *Acta biomater.*, 2010, **6**, 756-62.

18 D. Wang, W. Liu, Q. Feng, C. Dong, Q. Liu, L. Duan, J. Huang, W. Zhu, Z. Li, J. Xiong, Y. Liang,

J. Chen, R. Sun, L. Bian and D. Wang, *Mater. Sci. Eng. C-Mater. Biol. Appl.*, 2017, **70**, 969-975.

19 O. Mahony, O. Tsigkou, C. Ionescu, C. Minelli, L. Ling, R. Hanly, M. E. Smith, M. M. Stevens and J. R. Jones, *Adv. Funct. Mater.*, 2010, **20**, 3835-3845.

20 G. J. Owens, R. K. Singh, F. Foroutan, M. Alqaysi, C. -M. Han, C. Mahapatra, H. -W. Kim and J. C. Knowles, *Prog. Mater. Sci.*, 2016, **77**, 1-79.

21 L. L. Hench and J. K. West, *Chem. Rev.*, 1990, **90**, 33-72.

22 D. Tian, P. Dubois, C. Grandfils, R. Jérôme, P. Viville, R. Lazzaroni, J. -L. Brédas and P. Leprince, *Chem.Mater.*, 1997, **9**, 871-874.

23 F. Baino, E. Fiume, M. Miola and E. Verné, *Int. J. Appl. Ceram. Technol.*, 2018, **15**, 841-860.

24 E. Norris, C. Ramos-Rivera, G. Poologasundarampillai, J. P. Clark, Q. Ju, A. Obata, J. V. Hanna, T. Kasuga, C. A. Mitchell, G. Jell and J. R. Jones, *Biomed. Mater.*, 2020, **15**, 015014.

25 W. Fan, X. Zhang and C. Li, *Compos. Commun.*, 2019, **15**, 68-75.

26 L. Che, Z. Lei, P. Wu and D. Song, *Adv. Funct. Mater.*, 2019, **29**, 1904450.

27 M. C. Matos, L. M. Ilharco and R. M. Almeida, *J. Non-Cryst. Solids*, 1992, **147-148**, 232-237.

28 R. H. Glaser, G. L. Wilkes and C. E. Bronnimann, *J. Non-Cryst. Solids*, 1989, **113**, 73-87.

29 M. A. Woodruff and D. W. Hutmacher, *Prog. Polym. Sci.*, 2010, **35**, 1217-1256.

30 S. -H. Rhee, *Biomaterials*, 2003, **24**, 1721-1727.

31 F. Tallia, L. Russo, S. Li, A. L. H. Orrin, X. Shi, S. Chen, J. A. M. Steele, S. Meille, J. Chevalier, P. D. Lee, M. M. Stevens, L. Cipolla and J. R. Jones, *Mater. Horizons*, 2018, **5**, 849-860.

32 N. Watanabe, S. Uemura and M. Okano, *Bull. Chem. Soc. Jpn.*, 1979, **52**, 3611-3614.

33 J. Pan, I. Hanna and J. -Y. Lallemand, *Tetrahedron Lett.*, 1991, **32**, 7543-7544.

34 L. Gabrielli, L. Connell, L. Russo, J. Jiménez-Barbero, F. Nicotra, L. Cipolla and J. R. Jones, *RSC Adv.*, 2014, **4**, 1841-1848.

35 T. To, L. R. Jensen and M. M. Smedskjaer, *J. Non-Cryst. Solids*, 2020, **534**, 119946.

36 M. Erol-Taygun, K. Zheng and A. R. Boccaccini, *J. Appl. Glass Sci.*, 2013, **4**, 136-148.

37 F. Rubio, J. Rubio and J. L. Oteo, *Spectrosc. Lett.*, 1998, **31**, 199-219.

38 P. Yu, R. J. Kirkpatrick, B. Poe, P. F. McMillan and X. Cong, *J. Am. Ceram. Soc.*, 2004, **82**, 742-748.

39 I. Artaki, M. Bradley, T. W. Zerda and J. Jonas, *J. Phys. Chem.*, 1985, **89**, 4399-4404.

40 L. S. Connell, F. Romer, M. Suarez, E. M. Valliant, Z. Zhang, P. D. Lee, M. E. Smith, J. V. Hanna and J. R. Jones, *J. Mater. Chem. B*, 2014, **2**, 668-680.

41 L. Abate, I. Blanco, G. Cicala, A. Mamo, G. Recca and Scamporrino, A. Scamporrino, *Polym. Degrad. Stab.*, 2010, **95,** 798.

42 M. Tanimoto, T. Yamagata, K. Miyata, and S. Ando, *ACS Appl. Mater. Interfaces* 2013, **5,** 4374.

43 W. C. Oliver and G. M. Pharr, *J. Mater. Res.*, 2011, **7**, 1564-1583.

44 E. Broitman, *Tribol. Lett.*, 2016, **65**, 23.

45 R. Arrigo and G. Malucelli, *Materials*, 2020, **13,** 2771

Table 1. Position (δ) and relative intensity (I) of the Q^n units in the different hydrolyzed structures. The results are obtained from the solid-state ^{29}Si MAS-NMR spectroscopy analysis.

Sample	Q^2		Q^3		Q^4	
	δ [ppm]	I [%]	δ [ppm]	I [%]	δ [ppm]	I [%]
$TEOS_1H_2O_{1.8}$	-92.3	5%	-101.7	43%	-110.9	52%
$TEOS_1H_2O_{3.6}$	-92.7	7%	-101.7	45%	-110.4	50%
$TEOS_1H_2O_{5.4}$	-92.3	7%	-101.7	44%	-110.6	49%

Table 2. Position and relative intensity of the T^n and Q^n units in the different hybrids with the same I/O ratio. The results are obtained from the solid-state ^{29}Si CPMAS-NMR spectroscopy analysis.

Sample	T^1		T^2		T^3		Q^3		Q^4	
	δ [ppm]	I [%]	δ [ppm]	I [%]	δ [ppm]	I [%]	δ [ppm]	I [%]	δ [ppm]	I [%]
$O_{0.7}I_{0.3}(T_1W_{1.8})$	-50.9	1	-60.0	17	-67.0	60	-102.5	7	-111.8	15
$O_{0.7}I_{0.3}(T_1W_{3.6})$	-50.5	1	-60.0	17	-66.9	63	-102.2	5	-111.4	14
$O_{0.7}I_{0.3}(T_1W_{5.4})$	-51.3	2	-59.5	15	-66.9	65	-102.3	3	-111.8	15
$O_{0.9}I_{0.1}(T_1W_{3.6})$	-50.5	3	-60.0	25	-67.1	61	-102.2	4	-111.2	7
$O_{0.4}I_{0.6}(T_1W_{3.6})$	-50.4	1	-59.4	13	-66.5	47	-102.4	14	-111.6	26

Table 3. The weight ratios of PCL/TEOS in the starting sol-gel reaction and the actual O/I wt% values measured from TGA processes.

Samples	PCL-diCOOH/TEOS wt%	Organic/Inorganic wt%
Org_1Inorg_0	100/0	86.7/13.3
$Org_{0.9}Inorg_{0.1}$	90/10	84.9/15.1
$Org_{0.8}Inorg_{0.2}$	80/20	79.6/20.4
$Org_{0.7}Inorg_{0.3}$	70/30	77.7/22.3
$Org_{0.6}Inorg_{0.4}$	60/40	73.3/26.7
$Org_{0.4}Inorg_{0.6}$	40/60	63.5/36.5

Table 4. Densities and Young's modulus of hybrids.

	$Org_{0.7}Inorg_{0.3}$ ($T_1W_{1.8}$)	$Org_{0.9}Inorg_{0.1}$ ($T_1W_{3.6}$)	$Org_{0.7}Inorg_{0.3}$ ($T_1W_{3.6}$)	$Org_{0.4}Inorg_{0.6}$ ($T_1W_{3.6}$)	$Org_{0.7}Inorg_{0.3}$ ($T_1W_{5.4}$)
Density (g cm^{-3})	1.235	1.216	1.237	1.287	1.237
Modulus (GPa)	0.86	0.54	1.15	1.68	1.29

Table 5. Hardness of hybrids from micro-indentation measurements.

	$Org_{0.7}Inorg_{0.3}$ ($T_1W_{1.8}$)	$Org_{0.9}Inorg_{0.1}$ ($T_1W_{3.6}$)	$Org_{0.7}Inorg_{0.3}$ ($T_1W_{3.6}$)	$Org_{0.4}Inorg_{0.6}$ ($T_1W_{3.6}$)	$Org_{0.7}Inorg_{0.3}$ ($T_1W_{5.4}$)
H (MPa)	5.0	2.6	9.1	58.8	7.0
Error	0.5	0.7	2.0	7.5	1.1

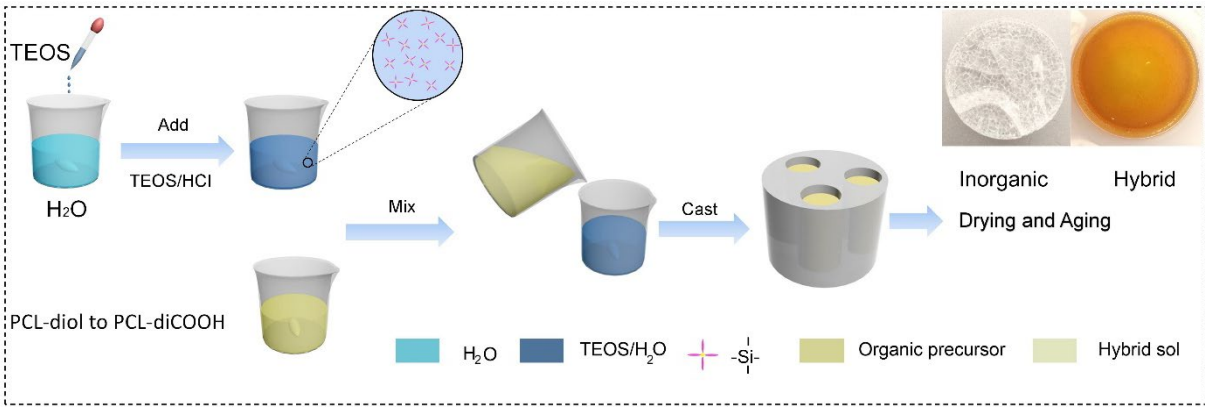

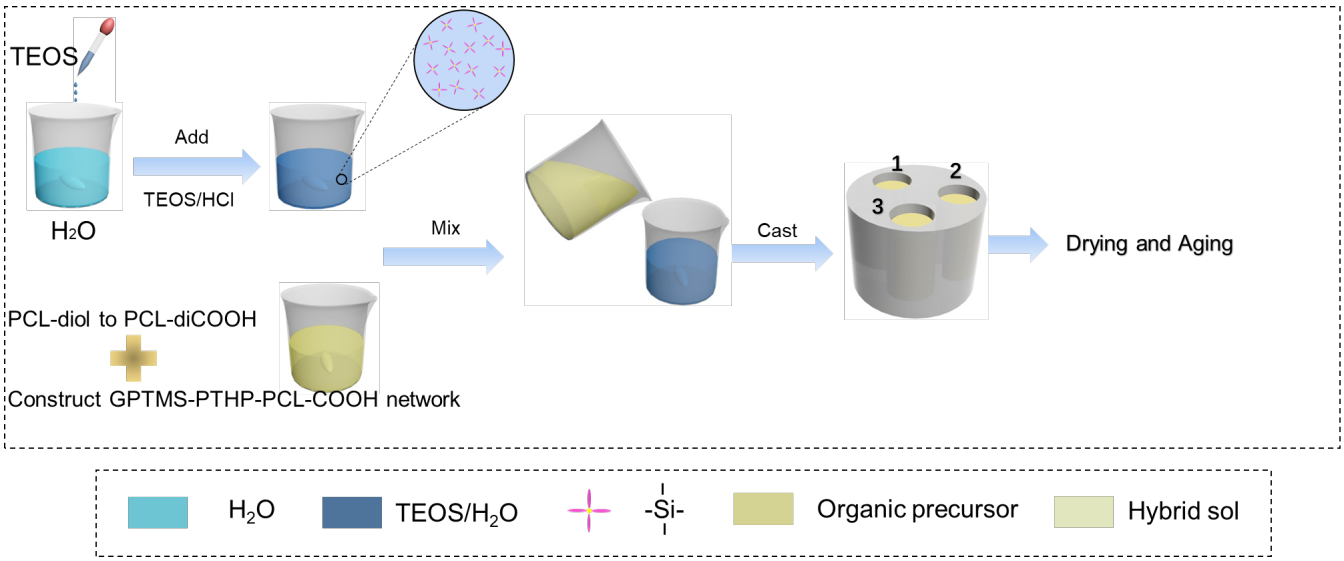

Scheme 1. The synthetic set-up and procedures of hybrids: casting, gelation, and aging and drying of merged sols from two pots of reactions for formation of silica-sol via hydrolysis of TEOS and organic sol by means of oxidation of HOOC-PCL-COOH and follow-up end-capping of GPTMS-PTHP (ring-opening polymerization of THP initiated by GPTMS).

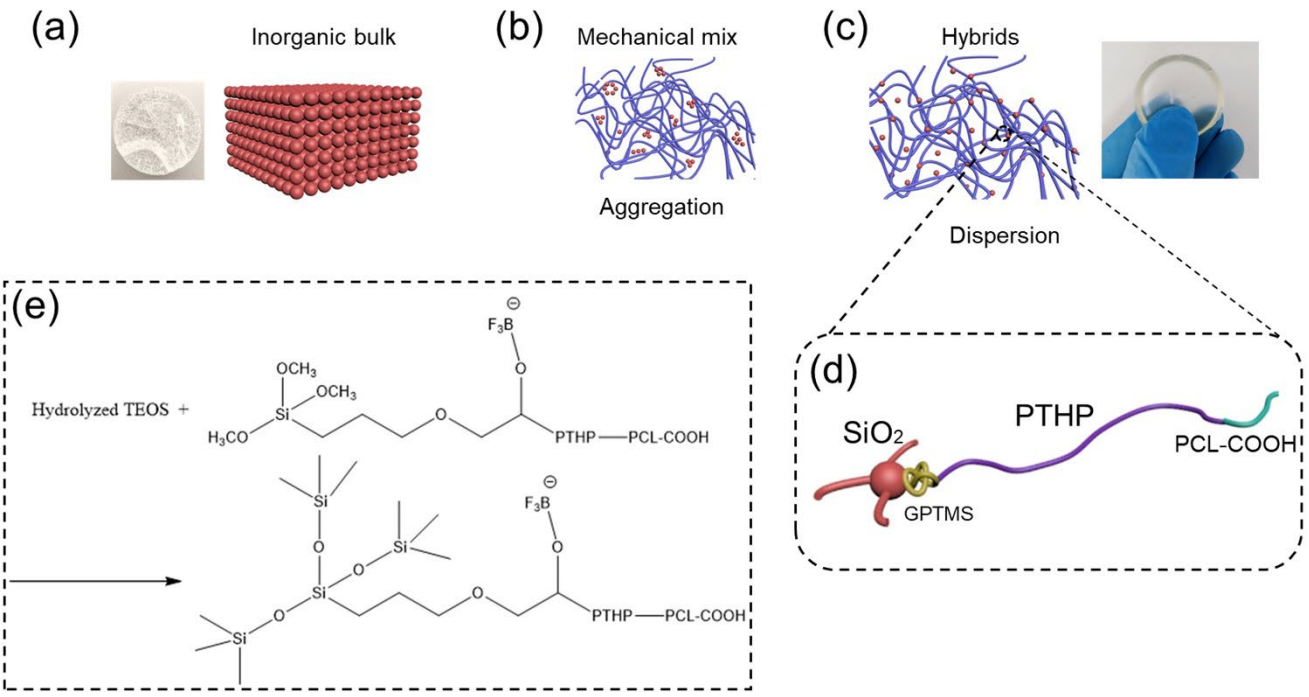

Fig. 1 Structural schemes of (a) inorganic bulk, (b) physically mixed hybrids, (c) covalently bonded hybrids, (d) covalent bonds between inorganic and organic parts, and (e) reaction process of precursors into hybrids.

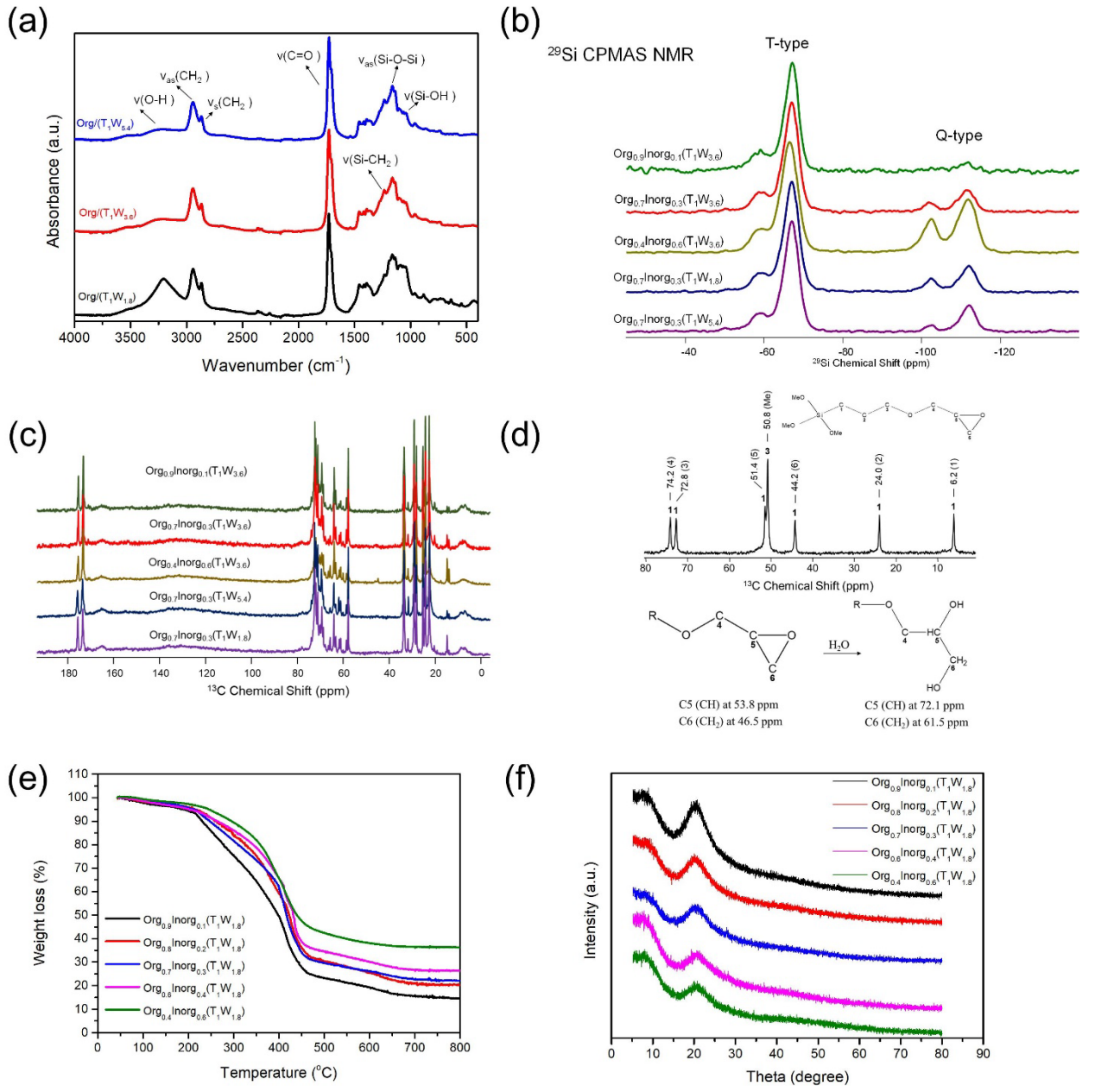

Fig. 2 (a) FT-IR spectra of hybrids with the same inorganic/organic (I/O) ratio but different TEOS/water (T/W) ratio. Solid state (b) ^{29}Si and (c) ^{13}C NMR spectra of hybrids with different compositions. (d) Hydrolysis of GPTMS and corresponding peak assignment of ^{13}C NMR spectrum. (e) TGA and (f) XRD spectra of hybrids with different I/O ratio.

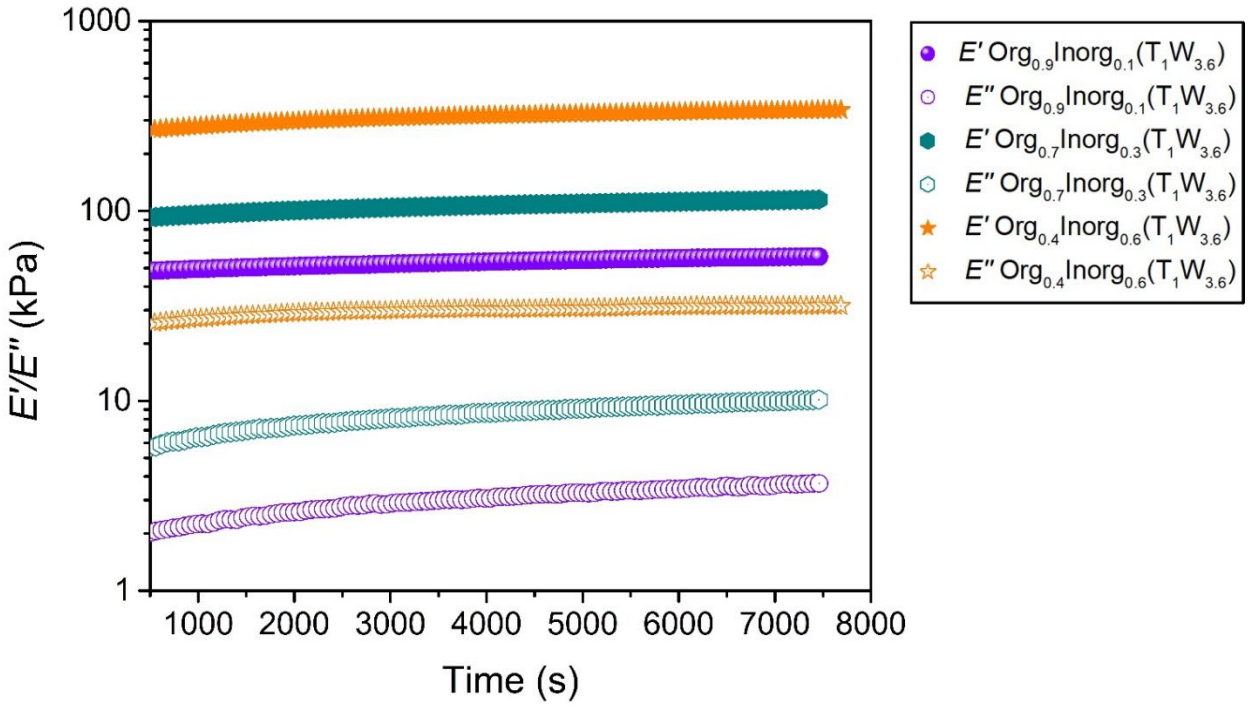

Fig. 3 Rheology properties: storage modulus (*E'*) and loss modulus (*E''*) as a function of time for hybrid $Org_{0.9}Inorg_{0.1}$ ($T_1W_{3.6}$), $Org_{0.7}Inorg_{0.3}$ ($T_1W_{3.6}$), and $Org_{0.4}Inorg_{0.6}$ ($T_1W_{3.6}$).

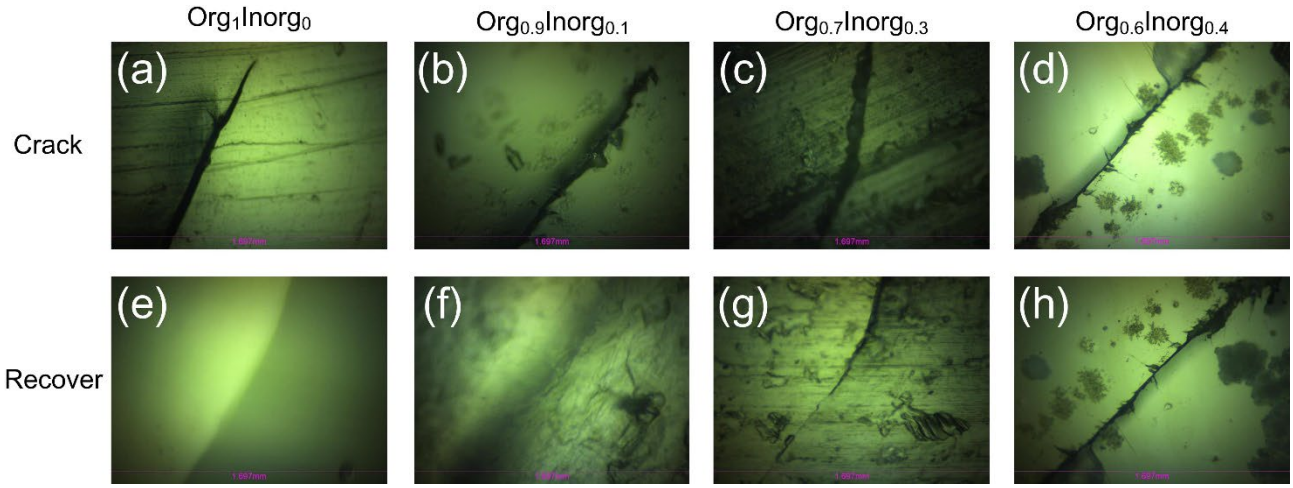

Fig. 4 Optical microscope images of four hybrid compositions after creation of a defect (top view) (a) Org_1Inorg_0; (b) $Org_{0.9}Inorg_{0.1}(T_1W_{1.8})$; (c) $Org_{0.7}Inorg_{0.3}(T_1W_{1.8})$; (d) $Org_{0.6}Inorg_{0.4}(T_1W_{1.8})$ and after self-healing for 24 hours (e) Org_1Inorg_0; (f) $Org_{0.9}Inorg_{0.1}(T_1W_{1.8})$; (g) $Org_{0.7}Inorg_{0.3}(T_1W_{1.8})$; (h) $Org_{0.6}Inorg_{0.4}(T_1W_{1.8})$.

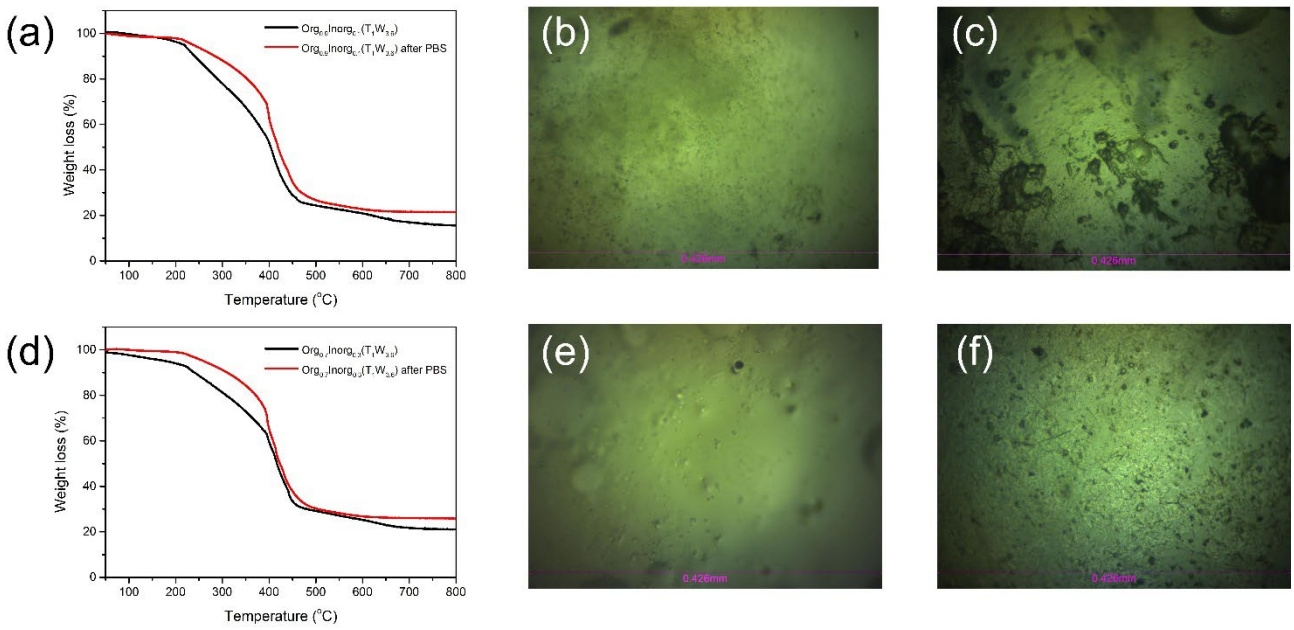

Fig. 5 (a) TGA of hybrid $Org_{0.9}Inorg_{0.1}(T_1W_{3.6})$ before and after immersed in PBS solution; optical microscope images of hybrid $Org_{0.9}Inorg_{0.1}(T_1W_{3.6})$, (b) before and (c) after immersed in PBS solution; (d) TGA of hybrid $Org_{0.7}Inorg_{0.3}(T_1W_{3.6})$ before and after immersed in PBS solution; optical microscope images of hybrid $Org_{0.7}Inorg_{0.3}(T_1W_{3.6})$, (e) before and (f) after immersed in PBS solution.